1932 *Inorg. Chem.* **2010**, *49*, 1932–1941
DOI: 10.1021/ic902351u

Inorganic Chemistry
Article

High-Frequency Electron Paramagnetic Resonance Analysis of the Oxidation State and Local Structure of Ni and Mn Ions in Ni,Mn-Codoped $LiCoO_2$

R. Stoyanova,*,† A.-L. Barra,‡ M. Yoncheva,† E. Zhecheva,† E. Shinova,† P. Tzvetkova,§ and S. Simova§

†*Institute of General and Inorganic Chemistry, Bulgarian Academy of Sciences, 1113 Sofia, Bulgaria,*
‡*Laboratoire National des Champs Magnétiques Intenses, CNRS, 38042 Grenoble Cedex 9, France, and*
§*Institute of Organic Chemistry with Centre of Phytochemistry, Bulgarian Academy of Sciences, 1113 Sofia, Bulgaria*

Received November 27, 2009

High-frequency electron paramagnetic resonance (HF-EPR) spectroscopy was employed to examine the oxidation state and local structure of Ni and Mn ions in Ni,Mn-codoped $LiCoO_2$. The assignment of EPR signals was based on Mg,Mn-codoped $LiCoO_2$ and Ni-doped $LiCoO_2$ used as Mn^{4+} and low-spin Ni^{3+} EPR references. Complementary information on the oxidation state of transition-metal ions was obtained by solid-state $^{6,7}Li$ NMR spectroscopy. For slightly doped oxides ($LiCo_{1-x}Ni_xMn_xO_2$ with $x < 0.05$), nickel and manganese substitute for cobalt in the CoO_2 layers and are stabilized as Ni^{3+} and Mn^{4+} ions. The local structure of Mn^{4+} ions was determined by modeling of the axial zero-field-splitting parameter in the framework of the Newman superposition model. It has been found that the local trigonal distortion around Mn^{4+} is smaller in comparison with that of the host site. To achieve a local compensation of Mn^{4+} charge, several defect models are discussed. With an increase in the total dopant content ($LiCo_{1-x}Ni_xMn_xO_2$ and $0.05 \leq x \leq 0.10$), a saturation in the Ni^{3+} amount (up to $x < 0.05$) is attained, while the Mn^{4+} content increases gradually. Ni^{3+} ions are surrounded by Co^{3+} ions only in the whole concentration range ($0 < x \leq 0.10$). The first metal coordination sphere of Mn^{4+} ions undergoes a transformation with an increase in the total Ni and Mn contents due to a progressive replacement of Co^{3+} by Mn^{4+} and Ni^{2+} ions. For highly doped oxides ($LiCo_{1-x}Ni_xMn_xO_2$ with $x = 0.10$), nickel and manganese achieve, with respect to the local charge compensation, their usual oxidation states of 2+ and 4+.

Introduction

Lithium cobaltates and lithium nickelates with the composition $LiMO_2$ (M = Co and Ni) are of significant research and technological interest as electrode materials for Li ion batteries because of their exceptional capability to intercalate reversibly large amounts of lithium at a potential of about 4 V.[1−3] The crystal structure of $LiMO_2$ (space group $R\bar{3}m$, α-$NaFeO_2$-type) is composed of consecutively arranged Li^+ and M^{3+} ions in the close-packed oxygen arrays, as a result of which discrete lithium and cobalt/nickel layers are formed.[4,5] The electrochemical reaction includes reversible Li^+ intercalation, which is concomitant with a reversible oxidation/reduction of Co/Ni^{3+} to Co/Ni^{4+} (one-electron reaction).[6,7] $LiCoO_2$ and $LiNiO_2$ form solid solutions in the whole concentration range ($LiCo_{1-x}Ni_xO_2$), thus providing opportunities to control precisely their electrochemical properties.[8−10]

Recently, $LiCo_{1-2x}Ni_xMn_xO_2$ compositions with $x = {}^1/_2$ and ${}^1/_3$ were proposed as the next generation of electrode materials.[11,12] In general, the layered crystal structure is preserved for $LiCo_{1-2x}Ni_xMn_xO_2$.[11,13] Contrary to $LiNiO_2$, Ni ions in $LiCo_{1-2x}Ni_xMn_xO_2$ are in the oxidation state 2+, while Co and Mn ions adopt their commonly found oxidation

*To whom correspondence should be addressed. E-mail: radstoy@svr.igic.bas.bg. Phone: +359 02 9793915. Fax: +359 02 8705024.

(1) Whittingham, M. S. *Chem. Rev.* **2004**, *104*, 4271–4301.
(2) Alcántara, R.; Lavela, P.; Tirado, J. L.; Zhecheva, R.; Stoyanova, R. *J. Solid State Electrochem.* **1999**, *3*, 121–134.
(3) Delmas, C.; Ménétrier, M.; Croguennec, L.; Levasseur, S.; Pérès, J. P.; Pouillerie, C.; Prado, G.; Fournès, L.; Weill, F. *Int. J. Inorg. Mater.* **1999**, *1*, 11–19.
(4) Orman, H. J.; Wiseman, P. J. *Acta Crystallogr.* **1984**, *40*, 12–14.
(5) Pouillerie, C.; Suard, E.; Delmas, C. *J. Solid State Chem.* **2001**, *158*, 187–197.
(6) Chen, Z.; Lu, Z.; Dahn, J. R. *J. Electrochem. Soc.* **2002**, *149*, A1604–A1609.
(7) Mansour, A. N.; McBreen, J.; Melendres, C. A. *J. Electrochem. Soc.* **1999**, *146*, 2799–2809.
(8) Delmas, C.; Saadoune, I. *Solid State Ionics* **1992**, *53−56*, 370–375.
(9) Zhecheva, E.; Stoyanova, R. *Solid State Ionics* **1993**, *66*, 143–149.
(10) Gross, T.; Buhrmester, Th.; Bramnik, K. G.; Bramnik, N. N.; Nikolowski, K.; Baehtz, C.; Ehrenberg, H.; Fuess, H. *Solid State Ionics* **2005**, *176*, 1193–1199.
(11) Lu, Z.; MacNeil, D. D.; Dahn, J. R. *Electrochem. Solid State Lett.* **2001**, *4*, A200–A203.
(12) Thackeray, M. M.; Johnson, C. S.; Vaughey, J. T.; Li, N.; Hackney, S. A. *J. Mater. Chem.* **2005**, *15*, 2257–2267.
(13) Lu, Z.; Chen, Z.; Dahn, J. R. *Chem. Mater.* **2003**, *15*, 3214–3220.

Published on Web 01/15/2010

states: 3+ and 4+, respectively.[14,15] As a result, the electrochemical reaction is a two-electron one, comprising a reversible oxidation of Ni^{2+} to Ni^{4+}, as well as Co^{3+} to Co^{4+}. The Mn^{4+} ions remain electrochemically inactive; their role is to stabilize the layered structure during the reversible electrochemical reaction.[12]

The common feature of all electrode compositions is the formation of separate layers comprising transition-metal and Li ions. The main difference between $LiCoO_2$ and $LiCo_{1-2x}Ni_xMn_xO_2$ comes from the short-range cationic distribution inside the transition-metal layers. This is a consequence of the appearance of cations with different ionic dimensions and oxidation states.[16−20] Using first-principles calculation, electron diffraction, high-resolution transmission electron microscopy and X-ray diffraction (XRD) analysis, solid-state ^{6}Li NMR, and Mn^{4+} electron paramagnetic resonance (EPR) experiments, a nonrandom cationic distribution has been established, which is consistent with Ni^{2+} and Mn^{4+} clustering.[16,17,19,20] On the contrary, a random Ni, Mn, and Co distribution in the layers has been reported by Whitfield et al. using neutron and anomalous dispersion powder XRD.[18]

Prior to the use of layered oxides as electrode materials, a detailed knowledge of the local structure and the oxidation state of the transition-metal ions is needed. EPR spectroscopy is a suitable experimental method for the study of both the electronic and geometric structures of transition-metal ions. Recently, enormous extension of the EPR capability was achieved because of application of a higher microwave frequency and a stronger magnetic field.[21] This technique is now recognized as high-frequency EPR (HF-EPR), which is operated at microwave frequencies and magnetic fields higher than 95 GHz and 3 T, respectively, whereas the conventional EPR is operated at 9.2 GHz and a magnetic field lower than 1 T (X-band EPR). For ions with $S = {}^1/_2$, HF-EPR allows resolution of a small **g**-tensor anisotropy, while for ions with an integer spin or $S > {}^1/_2$, the higher field employed here permits the precise determination of the axial and rhombic zero-field-splitting (ZFS) parameters.[21−23] In general, EPR parameters are determined mainly by spin−orbit coupling, as a result of which they are highly sensitive to small differences in the coordination sphere of the transition-metal ions.[21,23]

Layered oxides represent complex solid solutions where more than one paramagnetic ion is stabilized. Analysis of the local structure of these complex solid solutions is a difficult task. However, multifrequency EPR has been used for the structural characterization of both $LiNi_yCo_{1-y}O_2$ ($0 \leq y \leq 1$)[24−29] and $LiCo_{1-2x}Ni_xMn_xO_2$ ($x = {}^1/_3$ and ${}^1/_2$) compositions.[20,30−33] Although Ni^{2+}, Ni^{3+}, and Mn^{4+} are EPR-active, EPR signals only from Ni^{3+} and Mn^{4+} ions have been detected.[20,24−33] In layered oxides, Ni^{3+} ions adopt a low-spin configuration with $S = {}^1/_2$,[20,26] while Mn^{4+} ions are in a high-spin configuration with $S = {}^3/_2$.[30−33] The EPR parameters of both Ni^{3+} and Mn^{4+} ions display a dependence not only on their immediate environment but also on the nature of the atoms in the second metal coordination sphere. On the basis of analysis of HF-EPR spectra of low-spin Ni^{3+} ions used as spin probes in layered $LiAl_yCo_{1-y}O_2$ and $LiGa_yCo_{1-y}O_2$,[24−26] a local tetragonal distortion of Ni^{3+} ions is observed when they are located in a mixed $Co_{6-y}Al_y$ environment. The strength of the crystal field for Ni^{3+} increases gradually, and the extent of the tetragonal distortion shows a tendency to increase along the progressive replacement of Co by Al. For $LiCo_{1-2x}Ni_xMn_xO_2$ with $x = {}^1/_3$ and ${}^1/_2$, signals from Mn^{4+} ions having a different number of Ni^{2+} as metal neighbors are clearly resolved by HF-EPR.[20,30−33] It is worth mentioning that while the local structure of Ni^{3+} ions in layered oxides has been the subject of intensive studies by HF-EPR spectroscopy,[24−26,28] little work has been done on the structural characterization of Mn^{4+}.[34]

The aim of this contribution is to analyze the oxidation state and local structure of both Ni and Mn ions in Ni,Mn-codoped $LiCoO_2$ by applying HF-EPR. In $LiCo_{1-2x}Ni_xMn_xO_2$, Ni and Mn dopants are in small amounts ($0 \leq x \leq 0.10$) in order to suppress the magnetic interactions between them. To facilitate the assignment of EPR signals, Mg,Mn-codoped $LiCoO_2$ was used as a Mn^{4+} EPR reference. First, the EPR studies are focused on the local environment of Mn^{4+} in Mg,Mn-codoped $LiCoO_2$. Structural information about the Mn^{4+} site in layered oxides was based on modeling of the magnitude of the ZFS parameter in terms of the Newman superposition model (NSM).[35−37] Then, the EPR spectra of Mn^{4+} in Ni,Mn-codoped $LiCoO_2$ are analyzed. Complementary information on the oxidation state of transition-metal ions was obtained by solid-state ^{6,7}Li NMR spectroscopy. This technique has been shown to provide valuable information on the local environment of the Li

(14) Hwang, B. J.; Tsai, Y. W.; Carlier, D.; Ceder, G. *Chem. Mater.* **2003**, *15*, 3676–3682.
(15) Yoon, W.-S.; Grey, C. P.; Balasubramanian, M.; Yang, X.-Q.; Fischer, D. A.; McBreen, J. *Electrochem. Solid-State Lett.* **2004**, *7*, A53–A55.
(16) Koyama, Y.; Tanaka, I.; Adachi, H.; Makimura, Y.; Ohzuku, T. *J. Power Sources* **2003**, *119*−*121*, 644–648.
(17) Yabuuchi, N.; Koyama, Y.; Nakayama, N.; Ohzuku, T. *J. Electrochem. Soc.* **2005**, *152*, A1434–A1440.
(18) Whitfield, P. S.; Davidson, I. J.; Cranswick, L. M. D.; Swainson, I. P.; Stephens, P. W. *Solid State Ionics* **2005**, *176*, 463–471.
(19) Cahill, L. S.; Yin, S.-C.; Samoson, A.; Heinmaa, I.; Nazar, L. F.; Gward, G. R. *Chem. Mater.* **2005**, *17*, 6560–6566.
(20) Shinova, E.; Stoyanova, R.; Zhecheva, E.; Ortiz, G. F.; Lavela, P.; Tirado, J. L. *Solid State Ionics* **2008**, *179*, 2198–2208.
(21) Krzystek, J.; Ozarowski, A.; Telser, J. *Coord. Chem. Rev.* **2006**, *250*, 2308–2324.
(22) Anderson, K. K.; Schmidt, P. P.; Ketterle, B.; Strand, K.; Palmer, A.; Lee, S.-K.; Solomon, E. I.; Gräslund, A.; Barra, A.-L. *J. Biol. Inorg. Chem.* **2003**, *8*, 235–247.
(23) Hagen, W. R. *Coord. Chem. Rev.* **1999**, *192*, 209–229.
(24) Zhecheva, E.; Stoyanova, R.; Alcántara, R.; Tirado, J. L. *J. Phys. Chem. B* **2003**, *107*, 4290–4295.
(25) Stoyanova, R.; Zhecheva, E.; Alcántara, R.; Tirado, J. L. *J. Phys. Chem. B* **2004**, *108*, 4053–4057.
(26) Stoyanova, R.; Barra, A.-L.; Zhecheva, E.; Alcántara, R.; Ortiz, G.; Tirado, J. L. *Inorg. Chem.* **2009**, *48*, 4798–4805.
(27) Stoyanova, R.; Zhecheva, E.; Alcantara, R.; Lavela, P.; Tirado, J. L. *Solid State Commun.* **1997**, *102*, 457–462.
(28) Barra, A.-L.; Chouteau, G.; Stepanov, A.; Rougier, A.; Delmas, C. *Eur. Phys. J. B* **1999**, *7*, 551–562.
(29) Reynaud, F.; Ghorayeb, A. M.; Ksari, Y.; Menguy, N.; Stepanov, A.; Delmas, C. *Eur. Phys. J. B* **2000**, *14*, 551–562.
(30) Stoyanova, R.; Zhecheva, E.; Vassilev, S. *J. Solid State Chem.* **2006**, *179*, 378–388.
(31) Stoyanova, R.; Zhecheva, E.; Alcántara, R.; Tirado, J. L. *J. Mater. Chem.* **2006**, *16*, 359–369.
(32) Yoncheva, M.; Stoyanova, R.; Zhecheva, E.; Alcántara, R.; Ortiz, G.; Tirado, J. L. *J. Alloys Compd.* **2009**, *475*, 96–101.
(33) Yoncheva, M.; Stoyanova, R.; Zhecheva, E.; Alcántara, R.; Ortiz, G.; Tirado, J. L. *Electrochim. Acta* **2009**, *54*, 1694–1701.
(34) Duboc, C.; Collomb, M.-N. *Chem. Commun.* **2009**, 2715–2717.
(35) Newman, D. J. *Adv. Phys.* **1971**, *20*, 197.
(36) Newman, D. J.; Ng, B. *Rep. Prog. Phys.* **1989**, *52*, 699.
(37) Müller, K. A.; Berlinger, W.; Blazey, K. W. *Solid State Commun.* **1987**, *61*, 21–25.

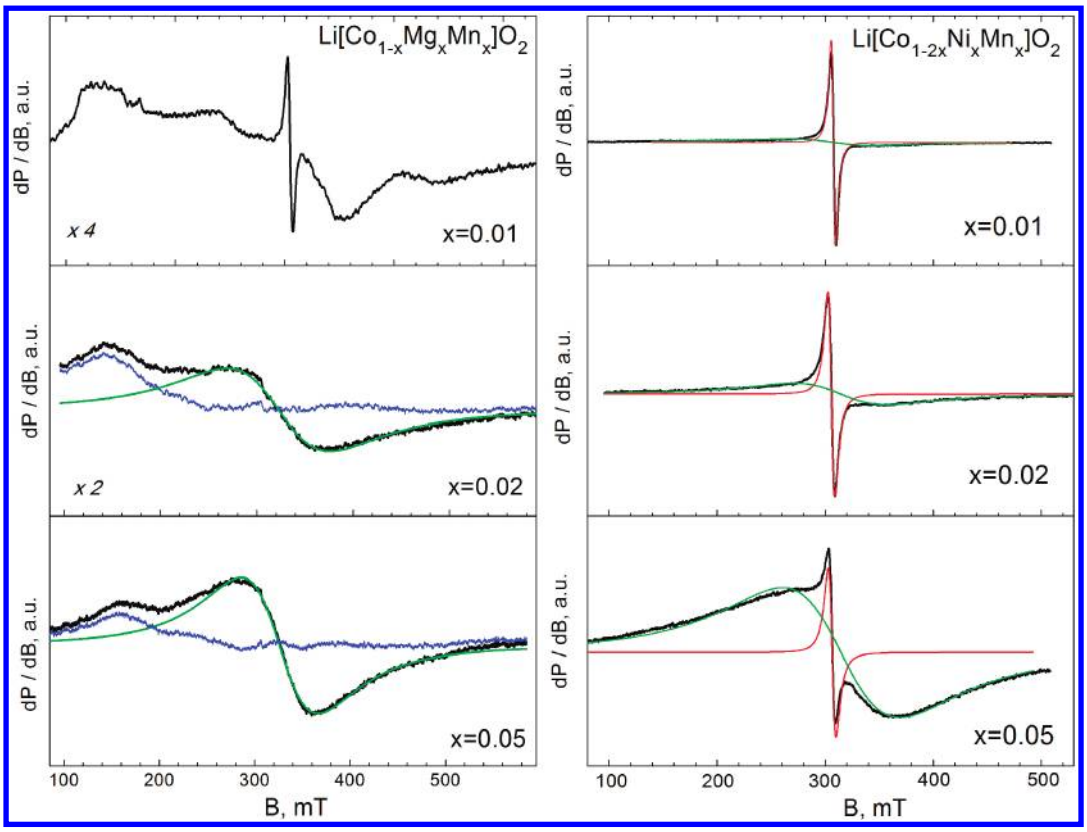

Figure 1. X-band EPR spectra at 103 K of $LiCo_{1-2x}Mg_xMn_xO_2$ (left) and $LiCo_{1-2x}Ni_xMn_xO_2$ (right). Black lines correspond to the experimental EPR spectra, red lines to the simulated signal due to low-spin Ni^{3+}, green lines to the simulated signal due to nonisolated Mn^{4+} ions, and blue lines to the signal due to isolated Mn^{4+} ions. For $LiCo_{0.98}Mg_{0.01}Mn_{0.01}O_2$, the narrow signal with $g = 2.14$ is due to Ni^{3+} impurities (concentrations of less than 0.001%). The intensity scales of $LiCo_{0.98}Mg_{0.01}Mn_{0.01}O_2$ and $LiCo_{0.98}Mg_{0.01}Mn_{0.01}O_2$ are magnified 4 and 2 times as compared to that of other samples.

nucleus in layered oxides because of 90° and 180° electron−nuclear interactions.[38−40]

Experimental Section

$LiCo_{1-2x}Ni_xMn_xO_2$ samples with $0 \le x \le 0.10$ were prepared by the coprecipitation method as described elsewhere.[20] This method relies on a solid-state reaction between coprecipitated cobalt, nickel, and manganese hydroxides and lithium hydroxides at 950 °C. Cobalt nitrate (Aldrich), which contains Ni, Mn, and Mg traces in concentrations of less than 10, 20, and 10 mg/kg, was used as a starting reagent. To compensate for the lithium volatility, an excess of 2.5% $LiOH.H_2O$ was used. For the sake of comparison, the same procedure was used for the preparation of $LiCo_{1-2x}Mg_xMn_xO_2$, where Mg^{2+} substitutes for Ni^{2+}. The single phase of $LiCo_{1-2x}Mg_xMn_xO_2$ was obtained in the concentration range of $0 \le x \le 0.05$.

The metal content of the samples was determined by atomic absorption analysis. The mean oxidation state of transition-metal ions was determined by iodometric titration.

X-ray structural analysis was made by a Bruker Advance 8 diffractometer with Cu Kα radiation. Step-scan recordings for structure refinement by the Rietveld method were carried out using $2\theta = 0.03°$ steps of 10 s duration. The computer program *FULLPROF* was used in the calculations.[41] In agreement with previous structural characterization,[13] the structural model used comprised lithium in 3b sites (0, 0, 0.5), $Co_{1-2x}Ni_xMn_x$ in 3a sites (0, 0, 0), and oxygen in 6c sites (0, 0, z) for the $R\bar{3}m$ space group. The Li/(Co + Ni + Mn) ratio was imposed by the chemical composition of the oxides. The refined structural parameters are as follows: $a = 2.8156$ Å, $c = 14.0508$ Å, and $z = 0.2594$ for $LiCoO_2$; $a = 2.8146$ Å, $c = 14.0641$ Å, and $z = 0.2602$ for $LiCo_{0.98}Ni_{0.01}Mn_{0.01}O_2$; $a = 2.8232$ Å, $c = 14.1062$ Å, and $z = 0.2609$ for $LiCo_{0.80}Ni_{0.10}Mn_{0.10}O_2$ obtained at 950 °C. For Mg,Mn-codoped $LiCoO_2$ (i.e., $LiCo_{0.90}Mg_{0.05}Mn_{0.05}O_2$), the refined structural parameters are $a = 2.8170$ Å, $c = 14.0974$ Å, and $z = 0.2592$.

EPR measurements at 9.23 GHz (X-band) were carried out in an ERS 220/Q spectrometer within the temperature range 85−410 K. The g factors were established with respect to a Mn^{2+}/ZnS standard. The HF-EPR spectra were recorded on a single-pass transmission EPR spectrometer built at the High-Magnetic Field Laboratory, Grenoble, France. The frequencies were varied from 95 to 345 GHz using Gunn diodes and their multipliers. The detection of absorption was performed with a bolometer. The recording temperatures were varied from 5 to 300 K using a variable-temperature insert (Oxford Instruments). The simulation software *SIM* written by Weihe was used to extract numerical values of spin Hamiltonian parameters from experimental EPR spectra.[42,43] The program is based on a full-matrix diagonalization procedure and allows the generation of powder pattern EPR spectra of spin systems with any values of the ZFS parameters relative to the operating frequencies. This program also takes into account the Boltzmann population factor in

(38) Marichal, C.; Hirschinger, J.; Granger, P.; Ménétrier, M.; Rougier, A.; Delmas, C. *Inorg. Chem.* **1995**, *34*, 1773.
(39) Grey, C. P.; Dupré, N. *Chem. Rev.* **2004**, *14*, 4493–4512.
(40) Zeng, D.; Cabana, J.; Bréger, J.; Yoon, W.-S.; Grey, C. P. *Chem. Mater.* **2007**, *19*, 6277–6289.
(41) Rodríguez-Carvajal, J. *Satellite Meeting on Powder Diffraction of the XV Congress of the IUCr*, **1990**; p 127.
(42) Glerup, J.; Weihe, H. *Acta Chem. Scand.* **1991**, *45*, 444.
(43) Weihe, H. *SIM software*; Institute of Chemistry, University of Copenhagen: Copenhagen, Denmark.

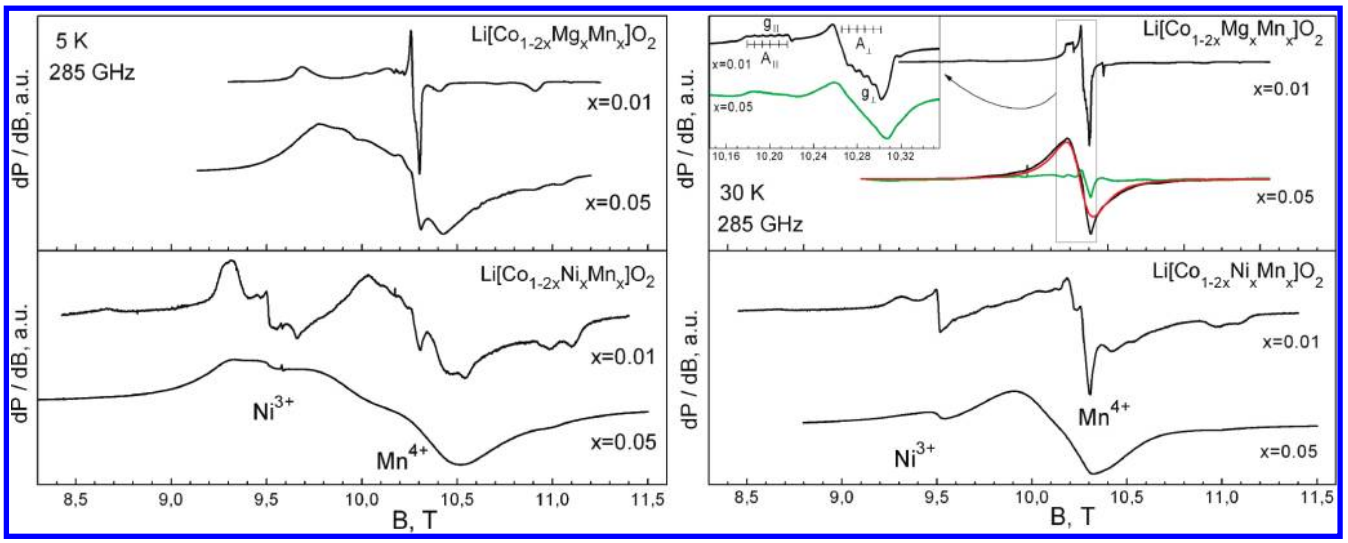

Figure 2. HF-EPR spectra at 285 GHz of $LiCo_{1-2x}Ni_xMn_xO_2$ and $LiCo_{1-2x}Mg_xMn_xO_2$. The temperatures of spectral recording are 5 and 30 K. Signals due to low-spin Ni^{3+}, isolated Mn^{4+}, and nonisolated Mn^{4+} ions (red line) are shown. The inset reveals details of the signal due to isolated Mn^{4+} ions: the signal with an axial symmetry ($g_{||} = 1.9968$, $g_{\perp} = 1.9765$, $A_{\perp} = 67.4 \times 10^{-4}$ cm^{-1}, and $A_{||} = 71.8 \times 10^{-4}$ cm^{-1}) for the slightly doped oxide ($x = 0.01$) and the asymmetric signal (obtained after subtraction of the simulated Lorentzian line from the experimental spectrum, green line) for the strongly doped oxide ($x = 0.05$).

calculating the EPR intensities. The Lorentzian line shape was used in the fitting procedure.

Solid-state [6,7] Li NMR spectra were recorded at 88.32 and 233.23 MHz (14.1 T) on a Bruker AV600II+ spectrometer. Magic-angle-spinning NMR spectra were recorded with single pulse excitation (1 μs) and a 0.2 s recycle delay. The number of scans acquired depended on the Li content of the sample, typically 128−1024 for ^{7}Li and 10 000−300 000 for ^{6}Li. The samples were loaded into 4 mm zirconia rotors and spun at 11.0 kHz. Chemical shifts are quoted in parts per million, from external tetramethylsilane (TMS; Ξ scale). The unified scale relies on Ξ values, stated as percentages $\Xi \equiv 100(\nu_X/\nu_{TMS})$, where ν_X is the absolute frequency for the 0 ppm position in the X spectrum and ν_{TMS} is the absolute frequency for ^{1}H NMR of TMS. The solid-state NMR spectra were fitted using *DMFIT* programs.[44]

Results

EPR Studies of Mn^{4+} Ions in Mg,Mn-Codoped $LiCoO_2$. The ground-state electronic term for Mn^{4+} in an octahedral crystal field is $^4A_{2g}$. When the symmetry is lowered in the absence of a magnetic field, the spin−orbit coupling induces a splitting of the spin sublevels into two Kramers doublets. The splitting between them is measured by the axial (D) and rhombic (E) ZFS parameters. The EPR features of Mn^{4+} depend on the D and E parameters. Two limiting cases are defined when the magnitude of the D parameter is either much larger or much smaller than $h\nu$. For accurate determination of the ZFS parameters, the use of multifrequency EPR is needed.

Figures 1 and 2 show the X-band and HF-EPR spectra of the Mn ions in Mg,Mn-codoped $LiCoO_2$. In the X-band experiment, the EPR spectrum of slightly doped oxides consists of multiple lines spanned over a wide field range: there are two sets of intensive lines with effective g values of 4.9 and 1.9 together with two other sets of low intensive lines with $g = 2.6$ and 1.5, respectively. All EPR lines are relatively broad, and the hyperfine structure is poorly resolved. When the Mn content increases, the multiple lines are further broadened. In general, the EPR patterns can be attributed to ions with $S > {}^1/_2$, for which the magnitude of the ZFS parameter is comparable with the energy of the microwave frequency ($h\nu \approx 0.3$ cm^{-1}, low-field approximation). However, the broad EPR lines cause difficulties in the detailed interpretation of the EPR spectrum detected in the X-band experiment. With an increase in the total dopant amount, an additional broad signal with a Lorentzian line shape, an isotropic g factor of 1.99, and a line width of 78 mT grows in intensity. The transformation of the multiple EPR lines into one symmetric line with an increase in the Mn content indicates that the broad signal comes from ions that are coupled by magnetic dipole−dipole and/or exchange interactions. These ions are usually denoted as nonisolated ions. The main conclusion from the X-band experiment is the presence of isolated and nonisolated paramagnetic ions in Mg,Mn-codoped $LiCoO_2$. To determine their origin, HF-EPR was undertaken.

The EPR profile undergoes a significant change when the microwave frequency increases (Figure 2). At 30 K, the HF-EPR spectrum (285 GHz) consists of a central signal with an axial symmetry. The values of the **g** tensor are $g_{||} = 1.9968$ and $g_{\perp} = 1.9765$. The signal displays a hyperfine structure with constants of $A_{\perp} = 67.4 \times 10^{-4}$ cm^{-1} and $A_{||} = 71.8 \times 10^{-4}$ cm^{-1}. The EPR parameters of the axially symmetric signal are typical for Mn^{4+} ions in oxide matrixes:[45] Mn^{4+} in Al_2O_3 with $g_{||} \cong g_{\perp} = 1.9937$ and $A_{||} \cong A_{\perp} = 70 \times 10^{-4}$ cm^{-1},[46] Mn^{4+} in h-$BaTiO_3$ with $g_{||} = 1.9901$ and $g_{\perp} = 1.9932$,[47] and Mn^{4+} in $PbTiO_3$ with $g_{||} = 1.997$ and $g_{\perp} = 1.985$.[48] This allows

(44) Massiot, D.; Fayon, F.; Capron, M.; King, I.; Le Calvé, S.; Alonso, B.; Durand, J.-O.; Bujoli, B.; Gan, Z.; Hoatson, G. *Magn. Reson. Chem.* **2002**, *40*, 70–76.

(45) Gatteschi, D.; Barra, A. L.; Caneschi, A.; Cornia, A.; Sessoli, R.; Sorace, L. *Coord. Chem. Rev.* **2006**, *11−12*, 1514–1529.

(46) Geschwind, S.; Kisliuk, P.; Klein, M. P.; Remeika, J. P.; Wood, D. L. *Phys. Rev.* **1962**, *126*, 1684–1686.

(47) Bottcher, R.; Langhammer, H. T.; Müller, T.; Abicht, H.-P. *J. Phys.: Condens. Matter* **2005**, *17*, 4925–4834.

(48) Laguta, V. V.; Glinchuk, M. D.; Bykov, I. P.; Maksimenko, Y. L.; Rosa, J.; Jastrabik, L. *Phys. Rev. B* **1996**, *54*, 12353–12360.

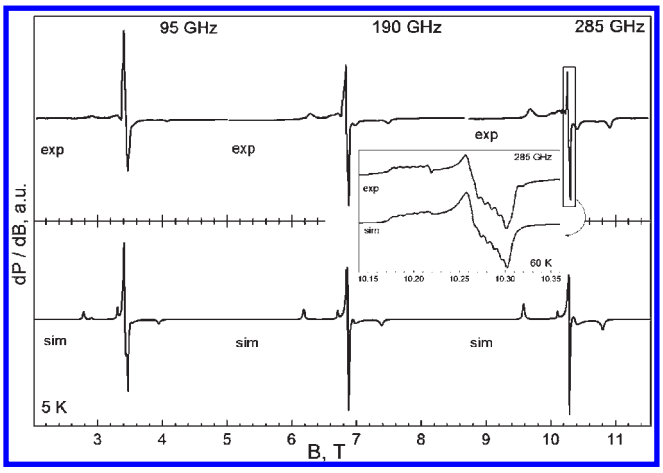

Figure 3. EPR spectra of Mg,Mn-codoped $LiCoO_2$ ($x = 0.01$). The spectra are registered at 95, 190, and 285 GHz. The experimental (exp) and simulated (sim) spectra are shown. The simulated spectra are generated by using the following EPR parameters: $g_{||} = 1.9968$ and $g_{\perp} = 1.9765$; $A_{\perp} = 67.4 \times 10^{-4}\,cm^{-1}$ and $A_{||} = 71.8 \times 10^{-4}\,cm^{-1}$; $D = -0.295\,cm^{-1}$ and $E/D = 0.247$.

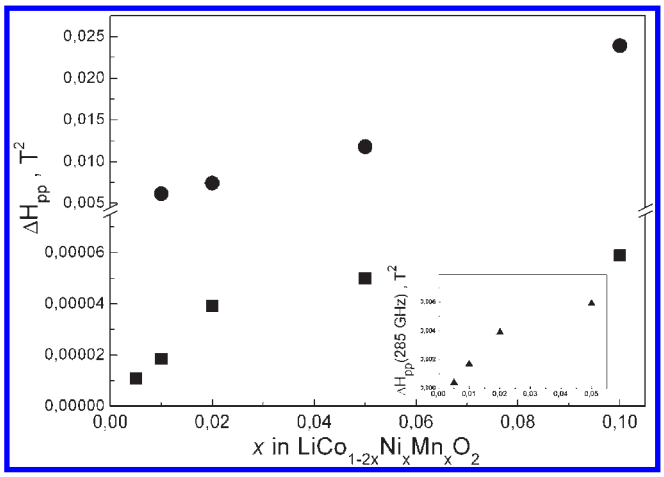

Figure 4. X-band EPR line width at 103 K of Ni^{3+} (■) and Mn^{4+} (●) as a function of the dopant content (x in $LiCo_{1-2x}Ni_xMn_xO_2$). The inset shows the EPR line width of Ni^{3+} (▲) determined at 285 GHz and 60 K.

assignment of the axially symmetric signal to Mn^{4+} with $S = {}^3/_2$. These ions are also responsible for the appearance of the multiple EPR spectrum in the X-band experiments.

When the temperature is lowered from 30 to 5 K, additional signals, which are shifted downfield and upfield to the central axial signal, become visible (Figure 2). Their intensities increase progressively at the expense of the central axial signal. At 5 K, two intensive outermost signals at about 9.6 and 10.9 T dominate the EPR spectrum. The temperature variation of the EPR patterns indicates that only one type of Mn^{4+} ion accounts for the EPR spectrum of $LiCoO_2$, which is slightly codoped Mg,Mn.

The structured EPR pattern of Mn^{4+} ions provides information on the splitting of the four magnetic sublevels of the ground state $S = {}^3/_2$ in a zero magnetic field (D and E, respectively). In the case when the microwave frequency exceeds the fine structure interactions (high-field approximation), the central signal corresponds to the $|-{}^1/_2\rangle$ to $|+{}^1/_2\rangle$ transition, while the outer lines come from the noncentral allowed transitions ($|\pm{}^3/_2\rangle$ to $|\pm{}^1/_2\rangle$, respectively). The line positions depend on both the magnitude of D and the E-to-D ratio, while the line intensities reflect the population of the M_S states.[22] As one can see, the high-field approximation is fulfilled when the EPR spectrum of Mn^{4+} in slightly codoped with Mg,Mn. $LiCoO_2$ is recorded at 285 GHz (Figure 2). The observed distance between the central line and the outermost line indicates that the D value has to be about 300 mT, while the line splitting is consistent with an E-to-D ratio slightly lower than 1:3. Using these values as the initial parameters, the powder EPR spectrum is generated by a simulation program written by Weihe.[42,43] By comparison of the generated EPR spectrum with the experimental one, the refined D and E parameters are determined: $D = -0.295\ cm^{-1}$ and $E/D = 0.247$ (Figure 3). The magnitude of the axial D parameter is comparable with that determined for Mn^{4+} in Al_2O_3, h-$BaTiO_3$, and $PbTiO_3$: $D = -0.1957\ cm^{-1}$, $|D| = 0.1160\ cm^{-1}$, and $|D| = 0.3157\ cm^{-1}$, respectively.[46−48]

To check the correctness of the experimentally obtained D and E parameters, EPR experiments at lower frequencies were undertaken. Figure 3 gives the Mn^{4+} EPR spectra registered at 95 and 190 GHz. Using the D and E values determined at 285 GHz, the same figure gives the simulated EPR spectra at these frequencies. As one can see, there is a satisfactory agreement between the experimental and simulated EPR spectra.

For highly Mg,Mn-codoped oxides, the HF-EPR spectrum at 30 K is a superposition of two signals with symmetric and axially symmetric shapes (Figure 2). The symmetric signal is well fitted by a Lorentzian line with a line width of 0.142 mT and a g value of 1.982 (Figure 2, red line). The g value of the Lorentzian line is close to the mean g value of the axially symmetric signal due to isolated Mn^{4+} ions in slightly doped oxides. This allows assignment of the broad Lorentzian signal to the nonisolated Mn^{4+} ions. After subtraction of the Lorentzian line from the experimental EPR spectrum, an axially symmetric signal with $g_{||} = 1.997$ and $g_{\perp} = 1.977$ is clearly visible (Figure 2, green line). These g values match that of isolated Mn^{4+} ions in slightly codoped oxides. This indicates that the axially symmetric signals detected for slightly and highly Mg,Mn-codoped oxides have one and the same origin. At 5 K, the EPR spectrum of the nonisolated Mn^{4+} ions becomes extremely broad because of magnetic dipole−dipole interactions (and/or magnetic exchange interactions). As a result, there are difficulties in the determination of ZFS parameters.

EPR Studies of Mn^{4+} Ions in Ni,Mn-Codoped $LiCoO_2$. The X-band EPR spectra of Mg,Mn- and Ni,Mn-codoped $LiCoO_2$ are compared in Figure 1. After replacement of Mg by Ni, two types of EPR signals become clearly resolved. A broad symmetric signal with a g factor of 1.99 dominates the EPR spectrum of highly doped $LiCo_{1-2x}Ni_xMn_xO_2$ oxides. The signal intensity decreases progressively when the dopant content decreases. In the same sequence, the line width also decreases (Figure 4). The signal possesses the same parameters as those in the case of Mg,Mn-substituted oxides. This allows assignment of the broad signal to nonisolated Mn^{4+} ions whose amount depends on the dopant content. Contrary to Mg,Mn-doped oxides, the signal due to

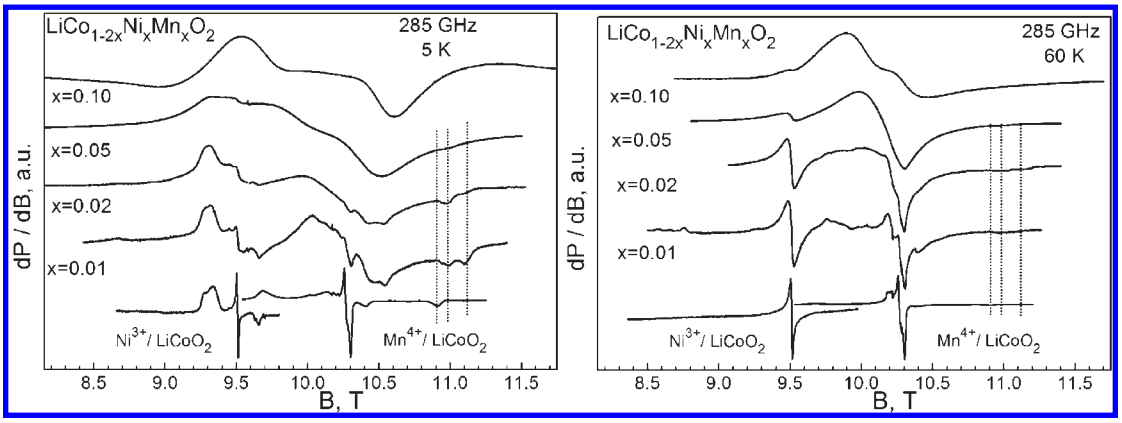

Figure 5. 285 GHz EPR spectra of $LiCo_{1-2x}Ni_xMn_xO_2$ with $x = 0.01$, 0.02, 0.05, and 0.10 at 5 and 60 K. EPR spectra for Ni^{3+} and Mn^{4+} references are also shown.

isolated Mn^{4+} ions is not detected in the X-band EPR spectra of Ni,Mn-doped oxides.

For slightly doped oxides, the EPR spectrum is dominated by the narrow signal with a Lorentzian line shape and a g factor of 2.14. The line width increases with the dopant content, reaching a nearly constant value of 9 mT at $x \approx 0.02$ (Figure 1). The signal intensity displays a complex dependence on the dopant content. There is an increase in the signal intensity up to $x = 0.02$, followed by a slight decrease: the relative intensities are 1.0. 2.1, 0.6, and < 0.1 for oxides with $x = 0.01$, 0.02, 0.05, and 0.10, respectively. The signal with the same g value and line width has been well documented for Ni^{3+}-doped $LiCoO_2$.[49,27] On the basis of EPR studies of layered $LiNi_xCo_{1-x}O_2$ solid solutions, the EPR signal is assigned to low-spin Ni^{3+} ions. From the concentration dependence of the EPR intensity and the line width, it is possible to determine the amount of Ni^{3+} ions in Ni, Mn-codoped $LiCoO_2$. It appears that, for slightly doped oxides ($x < 0.05$), all Ni ions adopt the oxidation state of 3+, whereas for highly doped oxides, Ni^{3+} reaches a constant value of about 0.05. Contrary to Ni^{3+} ions, Mn^{4+} ions increase proportionally with the Ni and Mn contents.

With a view to a more detailed analysis of the local structures and oxidation states of Ni and Mn ions, HF-EPR spectroscopy was undertaken (Figure 2). The two signals due to Ni^{3+} and Mn^{4+} ions are clearly detected in the EPR spectrum of $LiCo_{0.98}Ni_{0.01}Mn_{0.01}O_2$ at 285 GHz. At 60 K, Ni^{3+} ions give rise to a single Lorentzian line with $g = 2.14$, which upon cooling is split into an anisotropic doublet and a nearly symmetric single line in the central part (Figure 2). According to our previous EPR studies on Ni^{3+}-doped $LiAl_yCo_{1-y}O_2$,[49,24,25] the anisotropic doublets originate from the vibronic doublet ground state, while the single line can be assigned to an excited vibronic singlet and/or a relaxation-averaged singlet. It is of importance that the EPR parameters of the Ni^{3+} ions in pure $LiCoO_2$ and Ni,Mn-codoped $LiCoO_2$ are the same. Recently, we demonstrated that the metal ions included in the first coordination sphere induced a local distortion of the NiO_6 octahedron, which is monitored by the changes in the g value of Ni^{3+}.[24,25] The constancy in the EPR parameters of Ni^{3+} ions in pure $LiCoO_2$ and Ni,Mn-codoped $LiCoO_2$ reveals the same local coordination of Ni^{3+} ions; i.e., Ni^{3+} ions are surrounded by Co^{3+} ions only.

Because Mn^{4+} is an ion with $S = {}^3/_2$, the EPR spectrum is more complex because of the splitting of the four magnetic sublevels of the spin ground state in zero magnetic field. At 60 K, the Mn^{4+} ions cause the appearance of a signal with axial symmetry and g values $g_\perp = 1.9765$ and $g_{||} = 1.996$, respectively (Figure 5). The g values coincide with that determined for Mn^{4+} in Mg,Mn-codoped $LiCoO_2$. Upon cooling, several weaker signals that are symmetrically shifted downfield and upfield in comparison with the central anisotropic signal become visible. At 5 K, the upper-field signals at about 11.0 T dominate the EPR spectrum of Mn^{4+}. This signal is shifted in comparison with that of Mn^{4+} in Mg,Mn-codoped oxides, indicating an increase in the ZFS parameters of Mn^{4+} in Ni,Mn-doped oxides. The downfield-shift signal (probably at 9.6 T) is not resolved because it falls in the range where the signal of Ni^{3+} is visible.

The temperature dependence of the line position and line intensity permits the determination of the axial and rhombic ZFS parameters for Mn^{4+} ions in $LiCoO_2$ (Figure 6). This procedure is the same as that described for Mg,Mn-codoped $LiCoO_2$. Thus, the values of axial and rhombic ZFS parameters are as follows: $D = -0.366\ cm^{-1}$ and $E/D = 0.212$.

With an increase in the dopant content, the intensity of the Ni^{3+} signal decreases (Figure 5). For highly doped oxides ($x = 0.10$), the signal due to Ni^{3+} is hardly visible. As in the case of the X-band EPR, the line width (determined at 60 K) increases with the dopant content, reaching a constant value of about 76 mT at $x \leq 0.05$ (Figure 4, inset). The g factor of Ni^{3+} is the same for slightly and highly doped oxides. Irrespective of the fact that the Ni^{3+} content is saturated for highly doped oxides, it is worth mentioning that there are no signals due to Ni^{2+} ions in both X-band and HF-EPR experiments. This can be understood if we suppose that the ZFS parameter for Ni^{2+} in $LiCoO_2$ is significantly higher, thus preventing its observation. For Ni^{2+} ions coordinated by oxygen ligands, it has been found that the magnitude of the ZFS parameter varies in wide ranges: $-1.38\ cm^{-1}$ for Ni^{2+} in a Al_2O_3 matrix, $-3.5\ cm^{-1}$ for $Ni(H_2O)_6^{2+}$ in $NiSO_4 \cdot 7H_2O$; $-5.3\ cm^{-1}$ for Ni^{2+} in a $LiNbO_3$ matrix.[50,51]

(49) Angelov, S.; Friebel, C.; Zhecheva, E.; Stoyanova, R. *J. Phys. Chem. Solids* **1992**, *53*, 443–448.

(50) Petrosyan, A. K.; Mirzakhanyan, A. A. *Phys. Status Solidi B* **1986**, *133*, 315–319.

(51) Ono, K. *J. Phys. Soc. Jpn.* **1953**, *8*, 802.

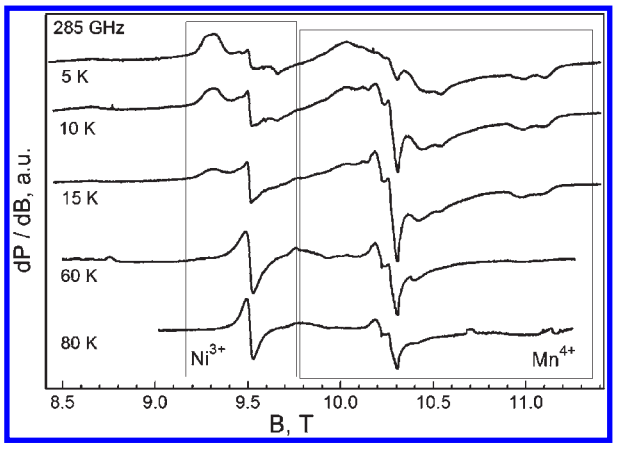

Figure 6. Temperature evolution of the EPR spectra (recorded at 285 GHz) of $LiCo_{0.98}Ni_{0.01}Mn_{0.01}O_2$ oxides. The signals due to low-spin Ni^{3+} and Mn^{4+} ions are indicated.

When the total Ni and Mn contents increase, there is a smooth conversion of the signal due to isolated Mn^{4+} ions into the signal due to nonisolated Mn^{4+} (Figure 6). The signal due to isolated Mn^{4+} is still visible for the oxide with $x = 0.05$, with the EPR parameters being the same. For this oxide ($LiCo_{0.90}Ni_{0.05}Mn_{0.05}O_2$), the EPR spectrum is dominated by the broad symmetric signal with $g = 1.982$, which is due to nonisolated Mn^{4+} ions. After a further increase in the dopant content ($LiCo_{0.8}Ni_{0.1}Mn_{0.1}O_2$), the EPR spectrum becomes more complex (Figure 6): the HF-EPR spectrum is a convolution of two nearly symmetric signals with g values of 1.981 and 2.024, respectively. The g value of the first signal ($g = 1.981$) matches the g value of nonisolated Mn^{4+}, while the g value of the second signal ($g = 2.024$) is slightly higher. The appearance of the two signals can be attributed to Mn^{4+} ions having different metal surroundings. Recently, it was found that each Ni^{2+} ion included in the first coordination sphere of Mn^{4+} leads to a progressive increase of the g value of Mn^{4+}.[20,30,31] It is noticeable that the dependence of the g value of Mn^{4+} on the number of Ni^{2+} neighbors has also been established for $LiMg_{0.5-x}Ni_xMn_{1.5}O_4$ spinels, where a long-range order between $Mg^{2+}{}_{1-2x}Ni^{2+}{}_{2x}$ and Mn^{4+} ions in the octahedral spinel sites takes place.[52,53] Therefore, the two symmetric signals can be assigned to Mn^{4+} ions having different local environments: (i) Mn^{4+} ions surrounded by Co^{3+} and identical Mn^{4+} ions (the signal with $g = 1.981$) and (ii) Mn^{4+} ions in an environment composed of Co^{3+}, Mn^{4+}, and one Ni^{2+} (the signal with $g = 2.024$). In the X-band experiment, the two signals merge into one broad signal. This broad signal is assigned to nonisolated Mn^{4+} ions (Figure 1).

^{6}Li and ^{7}Li NMR Spectra of Ni,Mn-Codoped $LiCoO_2$. Complementary to EPR spectroscopy, solid-state ^{6,7}Li NMR spectroscopy was used with the aim of analyzing the oxidation state of paramagnetic ions by probing the Li local environment. In pure $LiCoO_2$ (where Co is in the diamagnetic state), Li^+ occupies a trigonally distorted octahedron and displays a chemical shift close to 0. For $LiCo_{1-2x}Ni_xMn_xO_2$, the important piece of information comes from the interactions between the Li nucleus and an unpaired electron of Ni and Mn ions. On the basis of detailed NMR studies of electrode materials with layered and spinel structures, the shift of ^{6}Li caused by paramagnetic Mn^{4+}, Ni^{2+}, and Ni^{3+} ions has been determined:[38−40] +250 and −60 ppm for 90° and 180° bounded $Mn^{4+}-O-Li^+$ ions, respectively; −30 and +170 ppm for 90° and 180° $Ni^{2+}-O-Li^+$ configurations, and −15 and +110 ppm for 90° and 180° $Ni^{3+}-O-Li^+$ configurations. All of these interactions have an additive effect, leading to discrete changes of the chemical shift of Li after progressive replacement of diamagnetic Co^{3+} neighbors by different paramagnetic ions.

Figure 7 shows the ^{6}Li and ^{7}Li NMR spectra of $LiCo_{1-2x}Ni_xMn_xO_2$ compositions. Because of smaller quadrupole moments, the ^{6}Li NMR spectra are better resolved. However, both ^{6}Li and ^{7}Li NMR spectra can be deconvoluted into several resonance lines, with chemical shifts, independent of the dopant content. The main resonance appears in the NMR spectra of all samples at −0.1 ppm. The relative intensity of this resonance line decreases with an increase in the Ni and Mn contents (Table 1). In addition to the central signal, two downfield-shifted resonance lines at +3.5 and 9.0 ppm with intensities increasing with the Ni and Mn contents are detected. Additionally, the resonance lines become broader (Table 1). For oxides with $x > 0.01$, an upfield-shifted resonance line at about −13 ppm is clearly resolved in both the ^{6}Li and ^{7}Li NMR spectra. The relative intensity of this resonance line shows a tendency to decrease with an increase in the Ni and Mn contents. For highly doped oxides, an additional upfield-shifted resonance line at about −58 ppm grows in intensity. It should be noted that the resonance lines at higher field are broader in comparison with the central resonance line.

The resonance at −0.1 ppm can be assigned to Li located in a diamagnetic-only Co^{3+} environment, taking into account the NMR studies on $LiCoO_2$.[54,55] The presence of paramagnetic ion substitutes (such as Ni and Mn) for diamagnetic Co^{3+} in $LiCoO_2$ in the first and second coordination spheres of Li is responsible for the observed upfield shifts of the lines.[38−40] The chemical shift at −13 ppm could be assigned to Li^+ with one Ni^{3+} (90° $Ni^{3+}-O-Li^+$ configurations) in the first coordination sphere, while the presence of Mn^{4+} in the second coordination sphere of Li^+ is responsible for the signal at −58 ppm (180° $Mn^{4+}-O-Li^+$ configurations). It is worth mentioning that in the NMR spectra of Ni,Mn-codoped $LiCoO_2$ no resonance line indicates the presence of Ni^{2+} ions. This result is consistent with the EPR data on $LiCo_{1-2x}Ni_xMn_xO_2$. The origin of the upfield-shifted resonance lines remains unclear. Positive shift resonances have been reported for undoped $LiCoO_2$ obtained in excess of Li.[54,55] In this case, $LiCoO_2$ is capable of accommodating a small excess of Li in the Co layers by the creation of oxygen vacancies, thus leading to $Li_{1+t}Co_{1-t}O_{2-t}$ with $t \approx 0.04$.[55] The overstoichiometric

(52) Zhecheva, E.; Stoyanova, R. *Solid State Commun.* **2005**, *135*, 405–410.
(53) Alcántara, R.; Jaraba, M.; Lavela, P.; Tirado, J. L.; Zhecheva, E.; Stoyanova, R. *Chem. Mater.* **2004**, *16*, 1573–1579.
(54) Levasseur, S.; Ménétrier, M.; Shao-Horn, Y.; Gautier, L.; Audemer, A.; Demazeau, G.; Largeteau, A.; Delmas, C. *Chem. Mater.* **2003**, *15*, 348–354.
(55) Menetrier, M.; Carlier, D.; Blangero, M.; Delmas, C. *Electrochem. Solid State Lett.* **2008**, *11*, A179–A182.

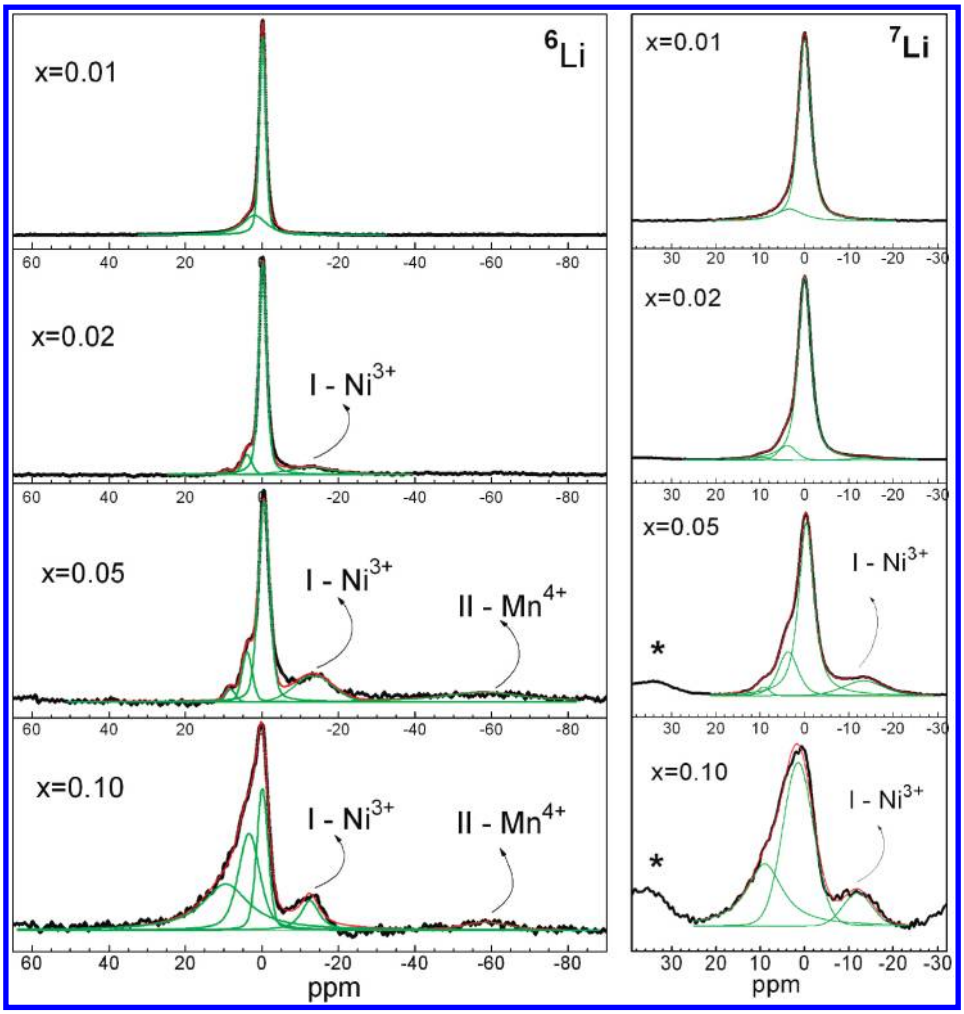

Figure 7. ^{6}Li and ^{7}Li NMR spectra (left and right) of $LiCo_{1-2x}Ni_xMn_xO_2$. The asterisk denotes the spinning side bands.

Table 1. Chemical Shifts (δ, ±0.05 ppm), Line Widths ($\Delta\delta$, ppm), and Relative Intensities of ^{6}Li NMR Signals in $LiCo_{1-2x}Ni_xMn_xO_2$

	signal 1			signal 2			signal 3			signal 4			signal 5		
	δ, ppm	$\Delta\delta$, ppm	A, au	δ, ppm	$\Delta\delta$, ppm	A, au	δ, ppm	$\Delta\delta$, ppm	A, au	δ, ppm	$\Delta\delta$, ppm	A, au	δ, ppm	$\Delta\delta$, ppm	A, au
x = 0.01	−0.2	1.97	0.71							2.0	7.4	0.29			
x = 0.02	−0.2	2.41	0.74				−13.0	13.8	0.16	3.9	3.0	0.08	9.2	2.1	0.02
x = 0.05	−0.4	3.48	0.49	−58	22.5	0.15	−13.0	12.0	0.18	3.9	3.1	0.12	8.2	2.9	0.06
x = 0.10	−0.2	3.52	0.21	−58	13.7	0.06	−13.0	5.64	0.08	3.4	6.6	0.29	9.5	14.7	0.36

$Li_{1+t}Co_{1-t}O_{2-t}$ displays downfield-shifted lines due to Li in different environments. In the spectra of the oxides studied by us, the intensities of the downfield-shifted lines increase with the Ni,Mn dopants, which allows association of their origin with long-range effects of Ni and Mn ions.

Discussion

Local Environment of Mn^{4+} Ions in Mg,Mn-Codoped $LiCoO_2$. Analysis of the local environment of Mn^{4+} is based on the modeling of the experimentally determined ZFS parameters. There are several mechanisms comprising the direct spin−spin interaction of the unpaired electrons and the spin−orbit coupling of the excited states with the ground state, which contribute to the ZFS parameters. In the analysis of the ZFS of transition-metal complexes, it is accepted that the contribution from the spin−spin coupling (SSC) is negligible and ZFS is mainly determined by spin−orbit coupling (SOC). The role of the SSC and SOC terms can now be calculated in the framework of the density functional theory (DFT)-based calculations.[56] For ions with d^3 and d^5 configurations, it has been demonstrated that the contribution of SSC is less than 30% of the total value of D.[57,58] It is worth mentioning that DFT calculations overestimate the importance of the spin−spin contribution and underestimate the spin−orbit terms. Irrespective of this fact, the DFT calculations predict that the D parameter coming from the SOC term is extremely sensitive toward the local environment of the transition-metal ions, while the SSC term is essentially geometry-independent.[58] Another

(56) Zein, S.; Neese, F. *J. Phys. Chem. A* **2008**, *112*, 7976–7983.
(57) Duboc, C.; Collomb, M.-N.; Pécaut, J.; Deronzier, A.; Neese, F. *Chem.—Eur. J.* **2008**, *14*, 6498–6509.
(58) Liakos, D. G.; Ganyushin, D.; Neese, F. *Inorg. Chem.* **2009**, *48*, 10572–10580.

method suitable for calculation of the ZFS parameters is the semiempirical NSM.[35,36,57] According to this model, the ZFS parameters are regarded as a superposition of the individual contributions of the separate neighboring ligands. The assumption is that the contribution of ligands is restricted toward the nearest neighbors and the interaction between the ligands is ignored. Despite these restrictions, the superposition model has been shown to provide valuable information on the local structure of transition-metal ions with d^3 and d^5 configurations.[59−63] The NSM expression for the ZFS parameters is as follows:[35,36,59]

$$b_2^0 = 3\sum_i \bar{b}_2(R_i)\, K_2^0(\Theta_i, \phi_i) \qquad (1)$$

where the fine-structure parameter (b_2^0) is related to the experimentally available axial ZFS: $D = b_2^0$. Here R_i is the distance between the ith ligand and the paramagnetic ion, Θ_i and ϕ_i are the polar and axial angles, and $K_2^0(\Theta_i,\phi_i)$ denotes the coordination factor that is specific for a particular geometrical arrangement. For a trigonal symmetry, $K_2^0(\Theta_i, \phi_i) = \frac{1}{2}(3\cos^2\Theta - 1)$.[35,36,59] The single ligand contribution is expressed by $\bar{b}_2(R_i)$, which is specific for a particular ion−ligand system and is determined by the nature of the ligand and the covalency of the bond. For Mn^{4+} ions coordinated by the oxygen ligand, the $\bar{b}_2(R)$ parameter has been derived from uniaxial stress experiments on Mn^{4+} in $SrTiO_3$:[37]

$$\bar{b}_2(R) = -A\left(\frac{R_0}{R}\right)^n + B\left(\frac{R_0}{R}\right)^m \qquad (2)$$

where $A = -11.1\ cm^{-1}$, $B = -8.48\ cm^{-1}$, $R_0 = 1.905$ Å, $n = 10$, and $m = 13$.

If Mn^{4+} occupies the trigonal host site, the D parameter can be expressed within the framework of the semiempirical superposition model as follows:

$$b_2^0 = 3\bar{b}_2(R)\,(3\cos^2\Theta - 1) \qquad (3)$$

where R is the Mn−O bond length and the trigonal distortion angle Θ stands for the angle between the Mn−O bond and the 3-fold axis (for the undistorted octahedron, the Θ value is 54.74°). For determination of the host $Co_{1-2x}Mg_xMn_x$−O bond length and the host trigonal angle Θ, the positions of the O atoms surrounding the Li and transition-metal ions in the layers were taken from the Rietveld refinement of powder XRD patterns of $LiCo_{1-2x}Ni_xMn_xO_2$. For the trigonal host site, the E parameter has to be zero.

From eq 3, one can conclude that the sign of D changes from negative to positive when the Mn^{4+} ions move from a trigonally compressed octahedron to a trigonally elongated octahedron. The experimentally determined D parameter of Mn^{4+} has a negative sign. This is evidence that Mn^{4+} occupies a trigonally compressed octahedron site in layered $LiCoO_2$. From a structural point of view, the negative sign of D reveals that Mn^{4+} substitutes for Co^{3+} ions in the CoO_2 layers, where a trigonally compressed host site is available.

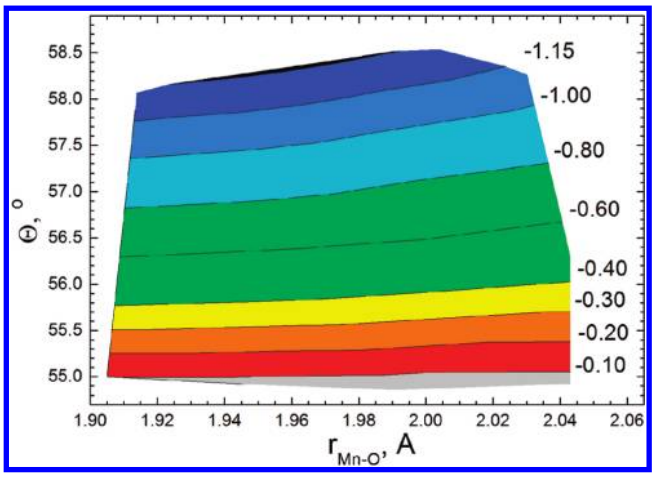

Figure 8. Dependence of the axial ZFS parameter (D) on the trigonal distortion angle (Θ) and the Mn−O bond length (r_{Mn-O}) calculated in the framework of the NSM.

Figure 8 presents the dependence of D on the Mn−O bond length and the trigonal angle. As one can see, the magnitude of the D parameter increases with the extent of trigonal distortion and with contraction of the Mn−O bond length. In $LiCo_{0.90}Mg_{0.05}Mn_{0.05}O_2$, the mean metal−oxide bond length and the trigonal distortion angle of the host site are 1.933 Å and 57.3°. If Mn^{4+} occupies the host site in $Co_{0.90}Mg_{0.05}Mn_{0.05}O_2$ layers, the magnitude of D has to be $-1.0\ cm^{-1}$. Comparison shows that the experimentally obtained D value is lower. This discrepancy indicates a local structural distortion around the Mn^{4+} ions located in the transition-metal layers. In lithium manganese oxides, Mn^{4+} usually adopts a bond length of about 1.90−1.94 Å.[64] These values are close to that determined for the host site in $Co_{0.90}Mg_{0.05}Mn_{0.05}O_2$ layers: 1.933 Å. If the bond length of Mn^{4+} in layered $LiCoO_2$ falls in the range of 1.90−1.94 Å, then the trigonal angle has to vary between 55.0 and 55.5°. This means that the local trigonal distortion around Mn^{4+} is smaller in comparison with the host trigonal distortion angle: 55.5 vs 57.4°.

Oxidation State and Local Structure of Ni and Mn in Ni, Mn-Codoped $LiCoO_2$. Going from Mg,Mn- to Ni,Mn-codoped $LiCoO_2$, the host site geometry is changed. The metal−oxygen bond length slightly decreases, together with an increase in the trigonal distortion angle: 1.924 Å and 57.9°, respectively. This is consistent with an increased magnitude of the D parameter of Mn^{4+} for Ni, Mn-codoped $LiCoO_2$. Supposing that Mn^{4+} occupies the host site in $Co_{0.80}Ni_{0.10}Mn_{0.10}O_2$ layers, the calculated D parameter would be significantly higher than the experimentally determined value: -1.2 vs $-0.366\ cm^{-1}$. The observed discrepancy indicates a local structural distortion around the Mn^{4+} ions. On the basis of the relationship of

(59) Siegel, E.; Müller, K. A. *Phys. Rev. B* **1979**, *20*, 3587–3596.
(60) Erdem, E.; Böttcher, R.; Gläsel, H.-J.; Hartmann, E. *Magn. Reson. Chem.* **2005**, *43*, S174–S182.
(61) Carmieli, R.; Larsen, T. M.; Reed, G. H.; Zein, S.; Neese, F.; Goldfarb, D. *J. Am. Chem. Soc.* **2007**, *129*, 4240–4252.
(62) Meštrić, H.; Eichel, R.-A.; Dinse, K.-P.; Ozarowski, A.; van Tol, J.; Brunel, L. C.; Kungl, H.; Hoffmann, M. J.; Schönau, K. A.; Knapp, M.; Fuess, H. *Phys. Rev. B* **2006**, *73*, 184105.
(63) Erdem, E.; Matthes, A.; Böttcher, R.; Gläsel, H.-J.; Hartmann, E. *J. Nanosci. Nanotechnol.* **2008**, *8*, 702–708.
(64) Strobel, P.; Lambert-Anderson, B. *J. Solid State Chem.* **1988**, *75*, 90.

the *D* parameter and the geometric structure of Mn^{4+} (Figure 8), the local structural distortion around the Mn^{4+} ions can be estimated: the trigonal distortion angle has to vary between 55.5 and 55.8° if the $Mn^{4+}-O$ bond length falls in the range of 1.90−1.94 Å. It is worth noting that the extent of trigonal distortion is still lower in comparison to the host distortion. The rhombic distortion seems similar for Mn^{4+} in both Mg,Ni- and Ni,Mn-codoped $LiCoO_2$ oxides.

For slightly Ni,Mn-codoped $LiCoO_2$ oxides, the Ni ions are preferentially stabilized as Ni^{3+}. These ions reside at the trigonal host site of transition-metal layers and are surrounded by Co^{3+} ions only. With an increase in the total dopant content, there is a saturation in the Ni^{3+} amount (up to $x \leq 0.05$), while the Mn^{4+} content increases gradually. Contrary to Ni^{3+} ions, the first metal coordination sphere of Mn^{4+} is smoothly changed with an increase in the total Ni and Mn contents: a progressive replacement of Co by Mn and Ni takes place. This means that, for highly Ni,Mn-codoped $LiCoO_2$ oxides, part of the Ni ions remain undetectable. The ion that is not detected by EPR in the layered oxides is Ni^{2+}.[20] This can be understood if the ZFS magnitudes for Ni^{2+} in the layered oxides are higher than 9 cm^{-1} (or 285 GHz). Although Ni^{2+} ions remain EPR-undetectable, they have an effect on the *g* values of Mn^{4+}: every Ni^{2+} in the first metal coordination sphere causes a discrete increase in the *g* values of Mn^{4+} (Figure 4). The appearance of Ni^{2+} ions in close proximity to Mn^{4+} ions should induce a significant chemical shift and line broadening of ^6Li and ^7Li nuclei, which prevents their observation by NMR experiments. In addition, the close location of both the Ni^{2+} and Mn^{4+} ions meets the requirements for local charge compensation. Therefore, for highly doped oxides, one can conclude that Ni and Mn adopt the oxidation states of 2+ and 4+.

The question is, how is the local charge of Mn^{4+} compensated for when Ni adopts preferentially the oxidation state of 3+? Because there is no EPR signal due to Mn^{2+}, the charge compensation can be achieved either by the creation of vacancies in the transition-metal layers or by the introduction of Li^+. The mechanism is still unclear. However, one can expect that the local distortion of Mn^{4+} ions will be sensitive to the appearance of metal vacancies or Li^+ ions in its first metal coordination sphere. Recently, we have demonstrated the effect of metal neighbors on the ZFS parameters of Fe^{3+} ions in layered $LiCo_{1-y}Al_yO_2$ oxides:[26] the maximum trigonal distortion for the FeO_6 octahedron is achieved when the Fe^{3+} ions were surrounded by Al^{3+} only, while the Co^{3+} environment yields a rhombic distortion of the FeO_6 octahedron. The reduced extent of the trigonal distortion of Mn^{4+} can, most probably, be related to the appearance of Li^+ as metal neighbors. The origin of Li^+ in the transition-metal layers is a consequence of the excess of the Li salts used during the synthesis of layered oxides.

Conclusions

Co doping of $LiCoO_2$ with Ni and Mn leads to the stabilization of Ni^{3+}, Ni^{2+}, and Mn^{4+} in the CoO_2 layers. For $LiCo_{1-2x}Ni_xMn_xO_2$ with *x* varying between 0 and 0.1, the Ni^{3+} content reaches a maximum of about $x \leq 0.05$, while the Mn^{4+} content increases in the whole concentration range. Above $x > 0.05$, Ni^{2+} ions in addition to Ni^{3+} appear in close proximity to Mn^{4+}. Irrespective of the total Ni and Mn contents, the Ni^{3+} ions are surrounded by diamagnetic Co^{3+} ions only. With an increase in the total Ni and Mn contents, there is a progressive replacement of Co^{3+} by Mn^{4+} and Ni^{2+} in the first metal coordination sphere of Mn^{4+}. For highly doped oxides ($LiCo_{1-x}Ni_xMn_xO_2$ with $x = 0.10$), Ni and Mn achieve, with respect to the local charge compensation, the usual oxidation states of 2+ and 4+. The extent of trigonal distortion of the MnO_6 octahedron is limited as compared to that of the host site: the trigonal distortion angle varies between 55.5 and 55.8°, and the $Mn^{4+}-O$ bond length is in the range of 1.90−1.94 Å.

The results obtained demonstrate, on the one hand, the capability of HF-EPR in comparison with $^{6,7}Li$ NMR spectroscopy to probe the local structure of more than one transition-metal ion stabilized simultaneously in the layered oxides and not coupled by magnetic interactions. On the other hand, the new information on the local structures and the oxidation states of Ni and Mn is essential in order to give a reliable correlation between the composition and electrochemical properties of $LiCo_{1-2x}Ni_xMn_xO_2$-based cathode materials.

Acknowledgment. The authors are indebted to the National Science Fund of Bulgaria (Contract Ch1701/2007) for financial support. The use of a Bruker AV600II+ NMR spectrometer is supported by the Project Contract UNA-17/2005. The HF-EPR measurements carried out at the High Magnetic Field Laboratory in Grenoble, France, were supported by the European Commission within the sixth framework programme "Transnational Access-Specific Support Action" (Contract RITA-CT-2003-505474), "Access to research in very high magnetic field". Authors are grateful to the partial financial support from the National Centre for New Materials (DO-02-82/2008).